This document is downloaded from DR-NTU (https://dr.ntu.edu.sg) Nanyang Technological University, Singapore.

Offline health diagnosis of power device based on nonintrusive inductively coupled approach

Yang, Hui-Chen; See, Kye Yak; Simanjorang, Rejeki; Li, Kang Rong

2018

Yang, H.-C., See, K. Y., Simanjorang, R., & Li, K. R. (2018). Offline health diagnosis of power device based on nonintrusive inductively coupled approach. IEEE Journal of Emerging and Selected Topics in Power Electronics, 6(4), 2053-2059. doi:10.1109/JESTPE.2018.2811753

https://hdl.handle.net/10356/82261

https://doi.org/10.1109/JESTPE.2018.2811753

© 2018 IEEE. Personal use of this material is permitted. Permission from IEEE must be obtained for all other uses, in any current or future media, including reprinting/republishing this material for advertising or promotional purposes, creating new collective works, for resale or redistribution to servers or lists, or reuse of any copyrighted component of this work in other works. The published version is available at: https://doi.org/10.1109/JESTPE.2018.2811753

Downloaded on 18 Jul 2024 13:23:37 SGT

Offline Health Diagnosis of Power Device Based on Non-Intrusive Inductively Coupled Approach

Hui-Chen Yang[1], Kye Yak See[1], Rejeki Simanjorang[2] and Kang Rong Li[1]

[1] School of Electrical and Electronic Engineering, Nanyang Technological University, Singapore

[2] Applied Technology Group, Rolls-Royce Singapore Pte. Ltd., Singapore

Corresponding Author: Ms. Hui-Chen Yang

Address Nanyang Technological University School of EEE

Electrical Power System Integration Lab

South Spine S2-B6C-04

50 Nanyang Link, Singapore 639798

Tel +65-83567747

Fax N/A

E-mail HYANG011@e.ntu.edu.sg

[†] This paper has not been presented at a conference or published elsewhere.

ABSTRACT- Understanding the causes of a power device's defect plays a crucial role in failure and reliability analyses, and hence, the need of health diagnosis. Heath diagnosis involves the measurement of pre-defined electrical parameter of a power device under its usual operating condition and the analysis of its deviation from its norm. Instead of the conventional direct measurements of voltage and current waveforms in time-domain, this paper proposes a non-intrusive measurement method that measures the on-state impedance of a power device in frequency-domain. The proposed method eliminates direct electrical contact with the device-under-test (DUT) and it has the ability to detect the deviation of the on-state impedance from its norm for health diagnosis purpose.

KEYWORDS- Power devices, health diagnosis, inductive coupling, silicon carbide.

I. INTRODUCTION

Semiconductor power devices in a power conversion system are subject to continuous electrical and thermal stresses and therefore they are prone to failures [1-2]. Any unexpected failures of these power devices can lead to system downtime and incur unnecessary economic loss. Therefore, the ability to detect a power device's incipient abnormality due to either aging, electrical stress or defect is crucial. Such abnormality can be detected through changes in measureable parameters, such as on-state resistance and on-state voltage [3-5].

Conventional time-domain voltage or current waveforms measurement methods require direct electrical contacts to the device-under-test (DUT) to monitor its health status. They can be broadly classified into three types based on different application scenarios. The first type performs continuous online measurement on an in-service system with embedded heath diagnostic circuits for health monitoring purpose [6-7]. The second type conducts periodic offline measurements with specific test sequence [8-9]. The third type characterizes the DUT's parameters during or after reliability tests, such as accelerated power and temperature cycling tests [10-11]. Among them, on-state voltage is the most frequently chosen parameter for health diagnosis purpose, which usually requires carefully pre-designed circuits be integrated with the DUT for reliable and accurate measurement [12]. As the on-state resistance change is rather small as compared to the overall on-state impedance of the DUT, the change in the on-state voltage may not be easily noticeable, especially for DUT with low operating current [13]. Turn-off transient waveform has also been used as an indirect indicator of the DUT's defect. For examples, the increase in parasitic inductance caused by damaged bonding wires leads to higher voltage spikes during turn-off transition [13]; and the reduction in gate capacitance caused by long-term aging results in lower ringing voltage during turn-off transition [14]. However, the ringing phenomenon can also be strongly influenced by additional inductance of external routing conductors, making it difficult to judge whether there is a true defect in the DUT. The gate current is another time-domain parameter for defect detection based on the assumption that the defect changes the gate capacitance [15]. However, noticeable change in gate current only occurs if all the bonding wires of the emitter (or source) in the DUT are completely damaged, which is very rare.

In view of the above-mentioned challenges faced by the time-domain measurement methods, this paper proposes an alternative non-intrusive method based on a fully inductively coupled approach. By injecting a sinusoidal test signal into the DUT and monitors its response simultaneously, the on-state impedance of the DUT can be measured for any specific frequency range of interest. It can be shown later that the measured on-state impedance of the DUT

in frequency-domain provides more visible changes and insights for health diagnosis purpose. For experimental demonstration purpose, a silicon carbide (SiC) power MOSFET is selected as the DUT in this paper. It is mounted on a specially designed test fixture, where a sinusoidal test signal is induced and monitored through inductive probes. The proposed method fits well for health diagnosis of power devices after they have subjected to accelerated stress tests. This paper is organized as follows: Section II provides the background of the on-state equivalent circuit model of SiC power MOSFET. The non-intrusive inductively coupled method is described in Section III. Section IV presents the experimental results for diagnosis of the health status of the DUT and discusses their causes. Finally, Section V concludes this paper.

II. ON-STATE EQUIVALENT CIRCUIT MODEL OF SIC POWER MOSFET

The equivalent circuit model of the drain-to-source on-state impedance of a SiC power MOSFET is illustrated in Fig. 1 (a). L_g, L_d and L_s are the bonding wires' inductances of the gate, drain and source, respectively. R_g' is the total resistance of the internal and external gate resistances in series. The gate-to-drain and gate-to-source capacitances are indicated as C_{gd} and C_{gs}, respectively; and R_{dson} is the on-state resistance. By applying Δ-Y transformation, C_{gd}, C_{gs} and R_{dson} can be converted to Z_g, Z_d and Z_s, as shown in Fig. 1(b). For a sinusoidal steady-state signal of angular frequency ω, the on-state impedance can be expressed as:

$$Z_{SiC} = \left(j\omega L_d + Z_d\right) + \left(R'_g + j\omega L_g + Z_g\right) // \left(j\omega L_s + Z_s\right) \tag{1}$$

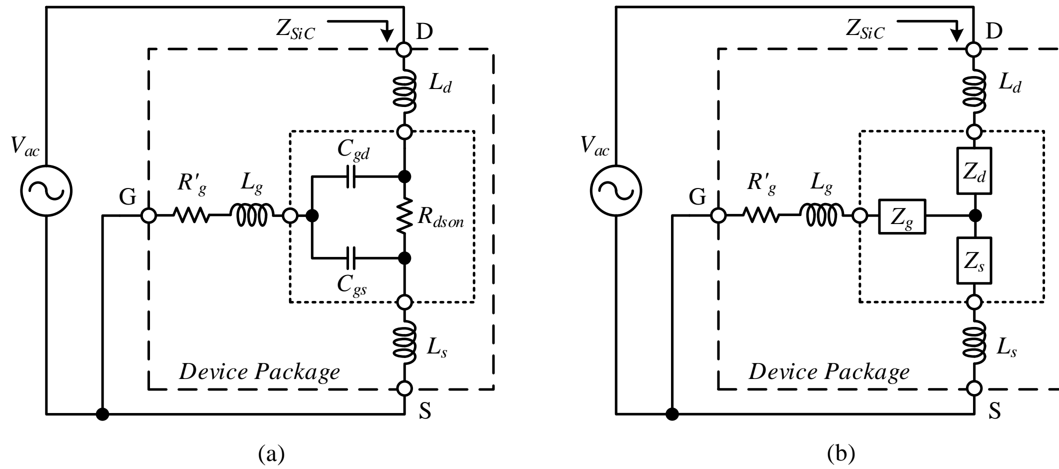

Fig. 1. (a) On-state equivalent circuit model of a SiC power MOSFET. (b) Equivalent on-state model of a SiC power MOSFET by converting C_{gd}, C_{gs} and R_{dson} to Z_g, Z_d and Z_s through Δ-Y transformation.

Z_g, Z_d and Z_s are determined by Δ-Y transformation:

$$Z_g = \frac{Z_{gd} Z_{gs}}{Z_{total}} \quad Z_d = \frac{Z_{gd} Z_{ds}}{Z_{total}} \quad Z_s = \frac{Z_{gs} Z_{ds}}{Z_{total}} \tag{2}$$

where $Z_{gd} = 1/(j\omega C_{gd})$, $Z_{gs} = 1/(j\omega C_{gs})$, $Z_{ds} = R_{dson}$ and $Z_{total} = Z_{gd} + Z_{gs} + Z_{ds}$.

$V_{DS} \approx 0$V when the MOSFET is at on-state, Z_g is usually >> Z_s within the frequency range of interest and $Z_g / Z_s = 1/(j\omega R_{dson} C_{gd})$. From the datasheet of the selected SiC power MOSFET (C2M0080120D, *Cree Inc.*) [16], $C_{gd} \approx 412$ pF and $R_{dson} = 80$ mΩ at 20 A rated current. Then, $|Z_g/Z_s| \approx 2.41\times10^2$ at 20 MHz, hence (1) can be simplified to:

$$Z_{SiC} \cong Z_d + Z_s + j\omega(L_d + L_s) \tag{3}$$

Substituting Z_d and Z_s from (2) into (3) gives:

$$Z_{SiC} = \frac{R_{dson}}{1 + j\omega R_{dson}(C_{gd} // C_{gs})} + j\omega(L_d + L_s) \tag{4}$$

From (4), it indicates that R_{dson} dominates in Z_{SiC} at low frequency and the inductive reactance of the bonding wires dominates in Z_{SiC} at high frequency. Using the generic packaged SPICE model of C2M0080120D provided by the manufacturer, the simulated $|Z_{SiC}|$ frequency response of a fully turn-on SiC power MOSFET with nominal $V_{GS} = 20$ V is plotted in Fig. 2. It shows the expected frequency response of the on-state impedance based on the earlier observation of (4). From the simulated frequency response of $|Z_{SiC}|$, Z_{SiC} can be modeled as a series RL circuit with $R = 69.2$ mΩ and $L = 15.5$ nH, as plotted together with the simulated response in Fig 2. In the frequency range of interest, the capacitive effects of C_{gd} and C_{gs} are insignificant. For more advanced power MOSFET with lower R_{dson} and higher C_{gd}, the upper frequency limit for the above simplification to be valid is expected to be lower.

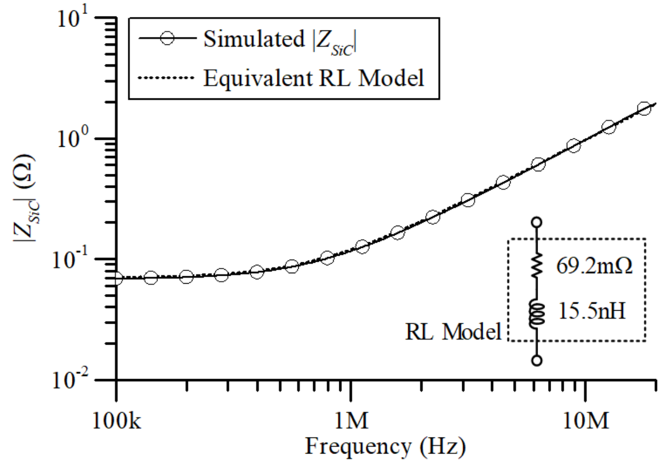

Fig. 2. Simulated frequency responses of the on-state impedance of the SiC power MOSFET (C2M0080120D) and its equivalent series RL model.

III. NON-INTRUSIVE INDUCTIVE COUPLING MEASUREMENT METHOD

A. Basic Principle

Inductive coupling method has been used for the extraction of in-circuit impedances of various circuits [17-20]. Further improvement for better measurement accuracy based on a two-port network model is reported in [20], which will be adopted in this paper. Fig. 3 shows the test setup to measure the unknown impedance Z_x of a DUT powered by a DC voltage. Two inductive probes, one for injecting and another for receiving, are clamped onto the wiring connection with a coupling capacitor C_c. Port 1 of the vector network analyzer (VNA) injects a sinusoidal signal into the circuit through an inductive probe. The injected signal flows into two paths, one into DC power supply and another into the DUT. It returns to the injecting point and is measured by port 2 of the VNA through another inductive probe. The injected signal amplitude can be increased for better signal to noise ratio, if needed. Z_s is the impedance of the power supply loop formed by the power supply V_{DC}, the biasing resistor R_b and the routing connections. Z_c is the resultant impedance of C_c and interconnections between nodes A and B. Hence, the actual impedance measured by the VNA is $Z = Z_c + Z_s//Z_x$. If $|Z_s| >> |Z_x|$, Z_x can be recovered by subtracting Z_c from Z.

The two-port network representation of Fig. 3 is shown in Fig. 4 with the currents and voltages of the respective ports clearly labeled. The overall two-port network M_{system} of the measurement setup seen by ports 1 and 2 of the VNA can be represented by three cascaded two-port networks. The first two-port network M_{inj} is the injecting probe clamped onto the circuit wiring, the second two-port network $M_{circuit}$ is the circuit itself and the last two-port network M_{rec} is the receiving probe clamped onto the circuit wiring. By adopting *ABCD* parameters representation for all the three two-port networks, the overall two-port network seen by the VNA is given by:

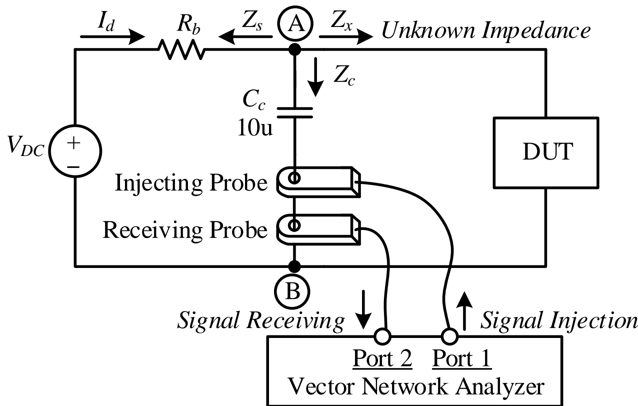

Fig. 3. Unknown impedance measurement setup based on inductive coupling method.

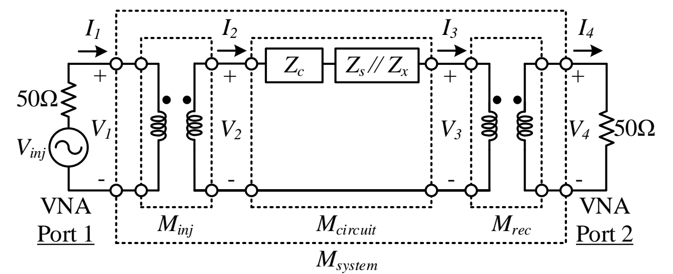

Fig. 4. Equivalent circuit model of the inductive coupling setup.

$$M_{system} = M_{inj} \cdot M_{circuit} \cdot M_{rec} \tag{5}$$

M_{inj} and M_{rec} can be obtained by characterizing each inductive coupling probe through measurement, which is well described in [20] and will not be repeated here. The *ABCD* parameters of each two-port network can be obtained by converting the measured *S*-parameters from the VNA as follows:

$$\begin{bmatrix} A & B \\ C & D \end{bmatrix} = \begin{bmatrix} \dfrac{1+S_{ii}-S_{jj}-S'}{2\cdot S_{ji}} & \dfrac{25\cdot\left(1+S_{ii}+S_{jj}+S'\right)}{S_{ji}} \\ \dfrac{1-S_{ii}-S_{jj}+S'}{100\cdot S_{ji}} & \dfrac{1-S_{ii}+S_{jj}-S'}{2\cdot S_{ji}} \end{bmatrix} \tag{6}$$

where the subscripts i and j represent the input and output ports of each two-port network, respectively [21]; and $S' = S_{ii}S_{jj} - S_{ij}S_{ji}$.

Finally, Z can be extracted from parameter B of $M_{circuit}$ by solving:

$$\begin{bmatrix} A & B \\ C & D \end{bmatrix}_{circuit} = \begin{bmatrix} A & B \\ C & D \end{bmatrix}_{inj}^{-1} \cdot \begin{bmatrix} A & B \\ C & D \end{bmatrix}_{system} \cdot \begin{bmatrix} A & B \\ C & D \end{bmatrix}_{rec}^{-1} \tag{7}$$

B. Experimental Validation

In the measurement setup shown in Fig. 3, R_b is chosen such that $|Z_s| >> |Z_x|$ in the frequency range of interest. It is chosen as 11.2 Ω to provide the DUT (SiC power MOSFET, P/N C2M0080120D) a biasing current of 1 A. The relatively low biasing current is chosen such that it avoids large variation in on-state resistance due to junction temperature change caused by heating, as well as to have low power dissipation in the biasing resistor. Though Z_c can be de-embedded from the impedance measured by the VNA, it is a good practice to minimize Z_c as much as possible so that Z_x, the impedance of the DUT dominates in the measurement. Two identical inductive coupling probes (Tektronix CT6) and a VNA (Rohde & Schwarz ZNB20 VNA) are selected for the experimental validation. Prior to the impedance measurement of the DUT, the measurement setup is validated with a few known precision surface-mounted device (SMD) type resistors with negligible parasitic. These resistors are treated as unknown impedance Z_x to be measured. Z is measured first and then the DUT is replaced with a short to obtain Z_c. $|Z_c|$ is well below 200 mΩ in the frequency range of interest as plotted in Fig. 5. Note that Z_c also includes inductive reactance of the wiring connections contributed by "node A $\rightarrow$ DUT $\rightarrow$ node B", which is much smaller than that contributed by "node A $\rightarrow C_c \rightarrow$ node B", as the connecting traces on the printed circuit board (PCB) is a lot shorter. Z_s is measured with the DUT removed. Finally, Z_c is subtracted from Z to obtain Z_x.

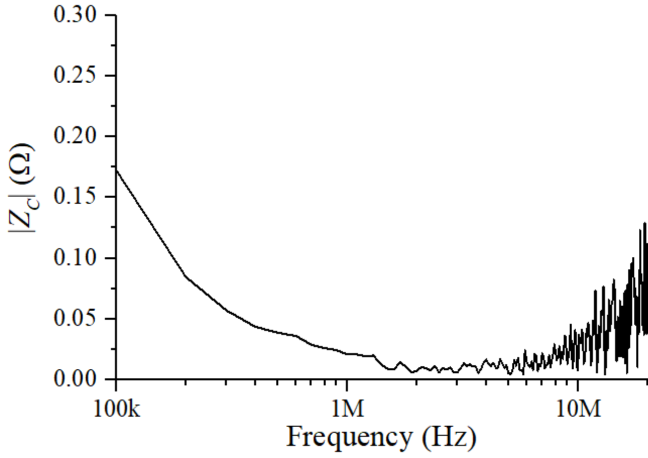

Fig. 5. Measured frequency response of $|Z_c|$.

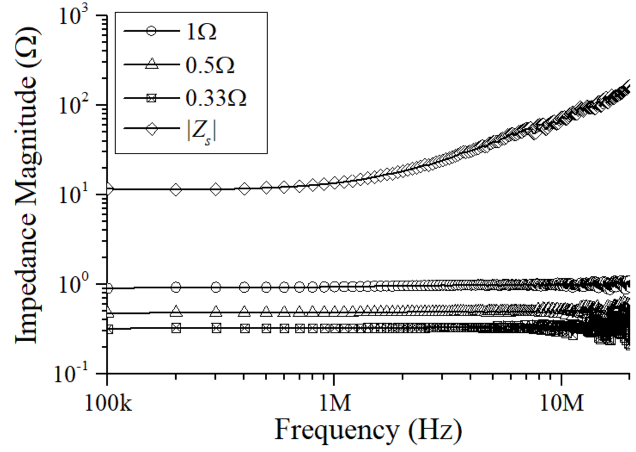

Fig. 6. Measured frequency response of resistors and $|Z_s|$.

Fig. 6 shows the measurement results of three resistors of small resistance for validation purpose. The standard precision resistors of 1 Ω with ± 1% tolerance are chosen. Two and three 1 Ω resistors are in parallel to give 0.5 Ω and 0.33 Ω resistances, respectively. The frequency response of $|Z_s|$ is also plotted in Fig. 6 to show that $|Z_s| >> |Z_x|$. The measured resistances using the proposed method agree reasonably well with the actual values. Next, a *RC* parallel circuit in series with *L* is chosen for further validation. This type of circuit is chosen to emulate the typical on-state impedance of a SiC power MOSFET, where R_{dson} dominates at lower frequency and the inductive reactance begins to surface at higher frequency. Again, both measured and simulated results are consistent with each other, as observed in Fig. 7.

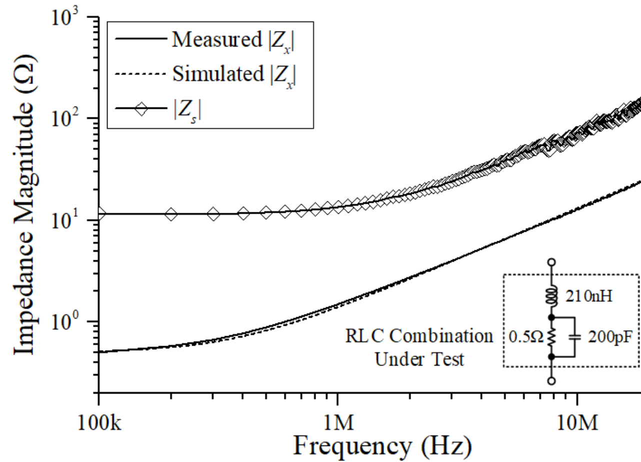

Fig. 7. Measured impedance frequency response of a parallel *RC* circuit in series with *L*.

IV. HEALTH DIAGNOSIS OF SIC POWER MOSFET

Based on the proposed method, the on-state impedance frequency response of the DUT is measured. Unless specified elsewhere, the DUT is fully turned on with a nominal gate bias voltage of 20 V. Fig. 8 shows the actual test fixture fabricated on a PCB. The terminal blocks are fix-mounted on the PCB for ease of DUT replacement between measurements so as to maintain similar environmental condition. Fig. 9 (a) shows the four similar DUTs to be measured. DUT-A and DUT-D are non-degraded power MOSEFTs with different pin length; DUT-B is a degraded power MOSFET after 20,000 temperature cycles, where the temperature cycling is achieved by repetitive change of the operating current between 24 A and 0.5 A to emulate the thermal stress, and the corresponding case temperatures are 35 °C and 27 °C, respectively; DUT-C is a non-degraded, de-capsulated power MOSFET with two of the bonding wires connected to the source terminal cut to emulate the defect. The impedance frequency responses of DUT-A and DUT-B are compared to evaluate the degradation of the DUT after the accelerated thermal stress. Since the pin leads of DUT-C have been cut during the de-capsulation process, its impedance frequency response will be compared with that of DUT-D for damaged bonding wire diagnosis. The images of DUT-C before and after the cutting of bonding wires are shown in Fig. 9 (b).

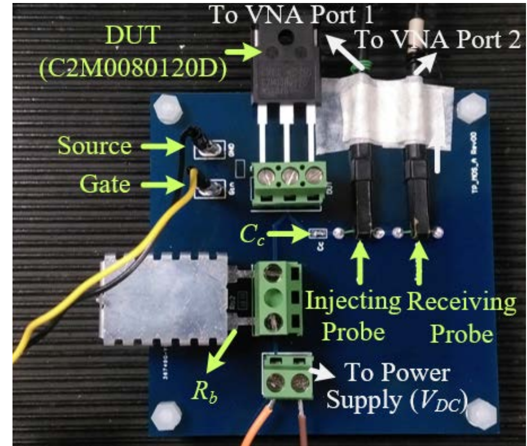

Fig. 8. Test fixture on PCB for health diagnosis of the SiC power MOSFET.

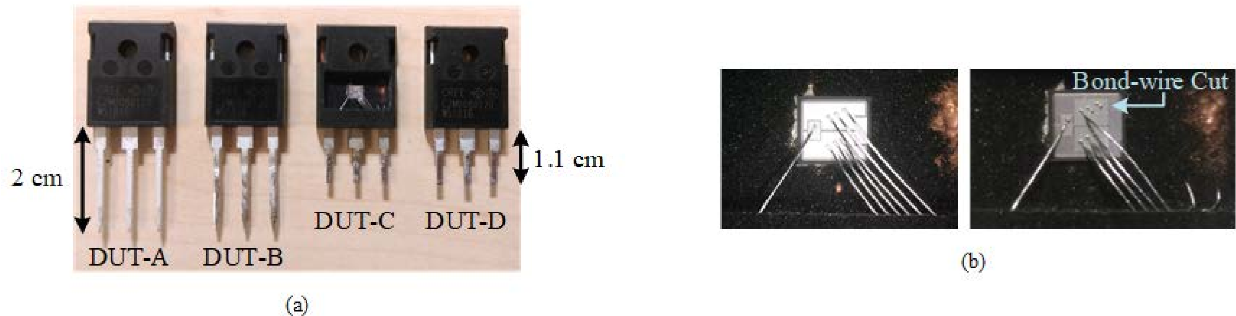

Fig. 9. (a) Four power MOSFETs to be measured. DUT-A: non-degraded, with pin length of 2 cm; DUT-B: degraded after 20,000 temperature cycles; DUT-C: non-degraded, de-capsulated with bonding wires damaged; DUT-D: non-degraded, with pin length of 1.1 cm. (b) Images of DUT-C before (the left image) and after (the right image) the cutting of bonding wires.

A. *Long-term Aging*

Fig. 10 shows the *I-V* characteristics of DUT-A and DUT-B measured with an *I-V* curve tracer (Tektronix 371A). It shows that R_{dson} of the degraded DUT-B deviates from its initial value by 29.1% at 10 A operating current. The on-state impedance frequency response measured with the proposed method at 1 A operating current is shown in Fig. 11. It clearly reveals the on-state resistance of the degraded DUT-B is higher than that of the non-degraded DUT-A. Table I compares the measured R_{dson} at DC using the *I-V* curve tracer and the measured $|Z_{SiC}|$ at 100 kHz using the proposed method at 1 A operating current. The frequency of 100 kHz is chosen for the proposed method, as the inductive effect is insignificant so that $|Z_{SiC}|$ is still dominated by the on-state resistance R_{dson}. The measured R_{dson} from *I-V* curve tracer and the proposed method agree well, with R_{dson} of the degraded DUT increased by 25% and 23%, respectively.

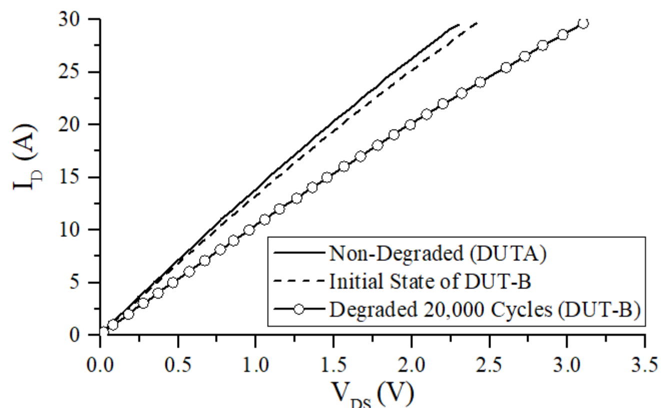

Fig. 10. *I-V* characteristics of DUT-A and DUT-B.

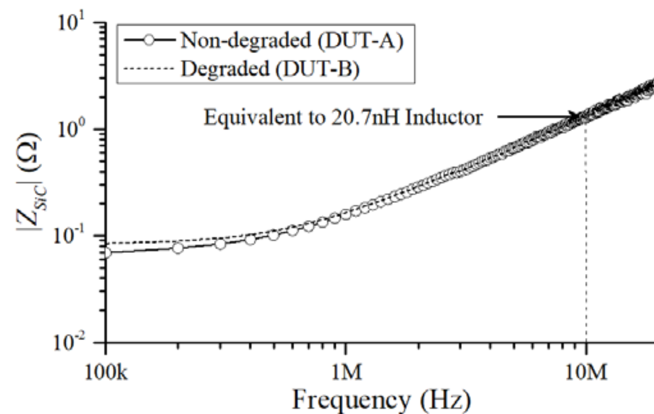

Fig. 11. On-state impedance frequency responses of DUT-A and DUT-B.

TABLE I

COMPARISON OF R_{dson} BY DIFFERENT METHODS

Measurement Method	R_{dson} (mΩ) @ 1A, Room Temperature	
	DUT-A	DUT-B (Degraded)
I-V Curve Tracer	64.0	80.0
The Proposed Method	68.8	84.4

B. *Loss of Gate Control*

Proper gate biasing voltage for a power MOSFET is essential for optimal operation in a power conversion system. Insufficient gate biasing voltage results in higher R_{dson}, which dissipates higher power and might consequently cause

thermal runaway. Fig. 12 illustrates that the proposed method has the ability to detect insufficient gate biasing voltage of DUT-A. The measured $|Z_{SiC}|$ at 100 kHz using the proposed method is dominated by R_{dson}, which agrees well with the calculated R_{dson} based on measured V_{DS} and I_D, as compared in Table II.

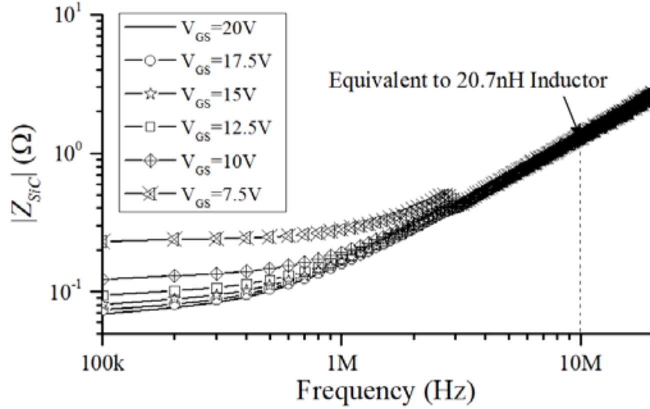

Fig. 12. On-state impedance frequency response of DUT-A with different gate biasing voltages.

TABLE II

MEASURED R_{dson} UNDER DIFFERENT V_{GS} BIASING

V_{GS} (V)	R_{dson} (mΩ) @ 1A, Room Temperature	
	Calculated from DC Measurement	The Proposed Method
20	67.3	68.8
17.5	72.9	73.8
15	80.2	80.7
12.5	92.4	94.4
10	120.5	123.2
7.5	225.3	229.7

C. Bonding Wire Damage

Bonding wires contribute a significant part of the parasitic inductance within a package. Z_{SiC} at higher frequency is dominated by inductive reactance and a power MOSEFT with damaged bonding wires is expected to exhibit higher inductive reactance at higher frequency. Fig. 13 shows the measurement results with and without damaged bonding wires. It clearly shows that the power MOSFET with damaged bonding wires exhibits higher inductive reactance as compared to that without damaged bonding wires. Based on the measured results, the extracted inductances are found to be 15.3 nH and 12.7 nH for DUT-C and DUT-D, respectively. For the case of damaged bonding wires, the time-domain methods may have difficulty to detect such defect, as the measurement is at DC. Hence, the merit of frequency-domain impedance measurement becomes apparent.

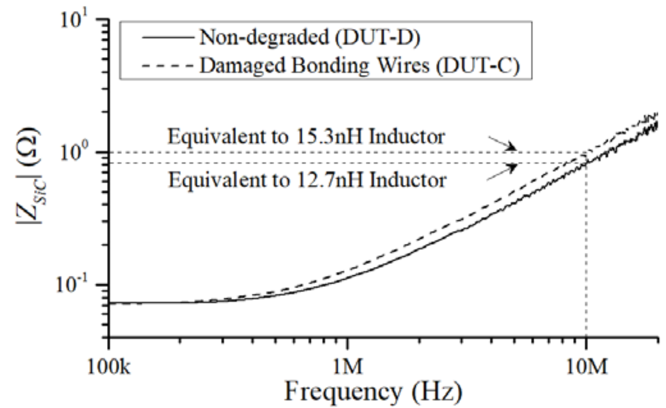

Fig. 13. On-state impedance frequency responses with and without damaged bonding wires.

V. CONCLUSION

Based on inductive coupling approach, a non-intrusive measurement method for the diagnosis of a SiC power MOSFET's health condition under its on-state operating condition has been described and validated. The ability of the proposed method to extract on-state impedance information in frequency-domain overcomes the shortcomings of the conventional time-domain based methods, as they are easily affected by the loading conditions and the system's noise. The proposed method does not require direct electrical contact with the DUT and therefore eliminates the safety hazards if the DUT operates at very high voltage. Using a selected power MOSFET as the DUT, it has demonstrated that by observing the impedance frequency response at both low and high frequencies, it is able to identify causes of on-state impedance variation, such as aging, damaged bonding wires, etc. Hence, the proposed method can be a useful mean for reliability and failure analyses. Further work will be carried out to replace the inductive coupling probes with carefully designed printed coils on the PCB so that the test fixture can be standalone and highly compact.

ACKNOWLEDGMENT

This work was conducted within the Rolls-Royce@NTU Corporate Lab with the support from the National Research Foundation (NRF) Singapore under the Corp Lab@University Scheme.

REFERENCES

[1] S. Yang, A. Bryant, P. A. Mawby, D. Xiang, L. Ran, and P. Tavner, "An industry-based survey of reliability in power electronic converters," *IEEE Trans. Ind. Appl.*, vol. 47, no. 3, pp. 1441–1451, May/Jun. 2011.

[2] H. Wang, M. Liserre, and F. Blaabjerg, "Toward reliable power electronics: challenges, design tools, and opportunities," *IEEE Industrial Electronics Magazine*, vol. 7, no. 2, pp. 17–26, Jun. 2013.

[3] M. Ciappa, "Selected failure mechanisms of modern power modules," *J. Microelectron. Rel.,* vol. 42, no. 4–5, pp. 653–667, Apr/May 2002.

[4] V. Smet, F. Forest, J. .J. Huselstein, F. Richardeau, Z. Khatir, S. Lefebvre and M. Berkani, "Ageing and failure modes of IGBT modules in high-temperature power cycling,"*IEEE Trans. Ind. Electron.*, vol. 58, no. 10, pp. 4931-4941, Oct. 2011.

[5] S. Dusmez, H. Duran and B. Akin, "Remaining useful lifetime estimation for thermally stressed power MOSFETs based on on-state resistance variation," *IEEE Trans. Ind. Appl.*, vol. 52, no. 3, pp. 2554–2563, May. 2016.

[6] J. M. Anderson and R. W. Cox, "On-line condition monitoring for MOSFET and IGBT switches in digitally controlled drives," in *Proc. IEEE Energy Conversion Congr. and Expo.*, Phoenix, AZ, 2011, pp. 3920–3927.

[7] P. Ghimire, A. Ruiz de Vega, S. Beczkowski, B. Rannestad, S. Munk-Nielsen and P. Thogersen, "Improving power converter reliability: Online monitoring of high-power IGBT modules," *IEEE Ind. Electron. Mag.*, vol. 8, no. 3, pp. 40–50, Sep. 2014.

[8] B. Ji, V. Pickert, W. Cao and B. Zahawi, "In situ diagnostics and prognostics of wire bonding faults in IGBT modules for electric vehicle drives," *IEEE Trans. Power Electron.*, vol. 28, no. 12, pp. 5568–5577, Dec. 2013.

[9] J. Due, S. Munk-Nielsen and R. Nielsen, "Lifetime investigation of high power IGBT modules," in *Proc. 14th European Conf. Power Electronics and Applications*, Birmingham, UK, 2011, pp. 1–8.

[10] D. C. Katsis and J. D. van Wyk, "Void-induced thermal impedance in power semiconductor modules: some transient temperature effects," *IEEE Trans. Ind. Appl.*, vol. 39, no. 5, pp. 1239–1246, Sep. 2003.

[11] S. Dusmez and B. Akin, "An accelerated thermal aging platform to monitor fault precursor on-state resistance," in *Proc. IEEE Int. Electric Machines and Drives Conf.*, Coeur d'Alene, ID, 2015, pp. 1–7.

[12] P. Ghirmire, S. Beczkowski, S. Munk-Neilson, B. Rannestad, and P. B. Thogerson, "A review on real time physical measurement techniques and their attempt to predict wear-out status of IGBT," in *Proc. 15th European. Conf. Power Electronics and Applications*, Lille, France, 2013, pp. 1–10.

[13] W. Kexin, D. Mingxing, X. Linlin, and L. Jian, "Study of bonding wire failure effects on external measurable signals of IGBT module," *IEEE Trans. Device Mater. Rel.*, vol. 14, no. 1, pp. 83–89, Mar. 2014.

[14] A. Ginart, M. Roemer, P. Kalgren, and K. Goebel, "Modeling aging effects of IGBTs in power drives by ringing characterization," in *IEEE Int. Conf. Prognostics and Health Management*, Denver, CO, 2008, pp. 1–7.

[15] S. Zhou, L. Zhou and P. Sun, "Monitoring potential defects in an IGBT module based on dynamic changes of the gate current," *IEEE Trans. Power Electron.*, vol. 28, no. 3, pp. 1479-1487, 2013.

[16] Cree Inc.," Silicon carbide power MOSFET C2M^{TM} MOSFET technology N-channel enhancement mode," C2M0080120D datasheet, Oct. 2015.

[17] R. A. Southwick and W. C. Dolle, “Line impedance measuring instrumentation utilizing current probe coupling,” *IEEE Trans. Electromagn. Compat.,* vol.13, no.4, pp.31–36, Nov. 1971.

[18] W. Y. Chang, W. S. Soh, K. Y. See and L. B. Wang, “Extraction of clock driver output impedance for signal integrity design,” *IEEE Trans. Electromagn. Compat.*, vol.53, no.4, pp.1034–1039, Nov. 2011.

[19] K. Li, A. Videt and N. Idir, “Multiprobe measurement method for voltage-dependent capacitances of power semiconductor devices in high voltage,” *IEEE Trans. Power Electron*., vol. 28, no. 11, pp. 5414–5422, Nov. 2013.

[20] K. R. Li, K.Y. See and X. M. Li, “Inductive coupled in-circuit impedance monitoring of electrical system using two-port ABCD network approach,” *IEEE Trans. Instrum. Meas.*, vol. 64, no. 9, pp. 2489–2495, Sep. 2015.

[21] D. M. Pozar, "Microwave network analysis," in *Microwave Engineering*, 2nd ed. New York, NY, USA: Wiley, 1998, ch. 4, pp.182–250.